J|A|C|S
ARTICLES
Published on Web 07/21/2006

Nanosphere and Nanonetwork Formations of [60]Fullerene-End-Capped Stereoregular Poly(methyl methacrylate)s through Stereocomplex Formation Combined with Self-Assembly of the Fullerenes

Takehiro Kawauchi,[†] Jiro Kumaki,*[,†] and Eiji Yashima*[,†,‡]

Contribution from the Yashima Super-structured Helix Project, Exploratory Research for Advanced Technology (ERATO), Japan Science & Technology Agency (JST), 101 Creation Core Nagoya, Shimoshidami, Moriyama-ku, Nagoya 463-0003, Japan, and Department of Molecular Design and Engineering, Graduate School of Engineering, Nagoya University, Chikusa-ku, Nagoya 464-8603, Japan

Received May 9, 2006; E-mail: kumaki@yp-jst.jp; yashima@apchem.nagoya-u.ac.jp

Abstract: We report a novel and versatile method for constructing a supramolecular nanosphere and nanonetwork based on isotactic and syndiotactic C_{60}-end-capped poly(methyl methacrylate)s (*it*- and *st*-PMMA-C_{60}'s) through their stereocomplex formation combined with self-assembly of the terminal C_{60}. The stereoregular PMMA-C_{60}'s with a precisely controlled structure including molecular weight, its distribution, tacticity, and the chain-end structure were synthesized by the stereospecific anionic living polymerizations of methyl methacrylate followed by end-capping with C_{60}, and their structures were proven by size exclusion chromatography, NMR, UV−vis, and MALDI-TOF-MS analyses. The stereoregular PMMA-C_{60}'s self-assembled to form a core−shell aggregate with C_{60} as the core and the PMMA chains as the shell in H_2O/CH_3CN (1/9, v/v) due to the solvophobic interaction of the C_{60} units. These *it*- and *st*-PMMA-C_{60} aggregates further supramolecularly assembled through iterative stereocomplex formation into nanonetworks in which the self-assembled C_{60} clusters were robustly connected with two- and three-dimensional arrangements. In addition, when the *it*- and *st*-PMMA-C_{60}'s were simultaneously mixed, self-assembly of the C_{60} units and stereocomplex formation of the *it*- and *st*-PMMA chains took place at once, resulting in the formation of uniformly sized spherical nanoparticles with resistance to heat. Similar nanonetwork architectures can be produced using *it*-PMMA-C_{60} clusters and *st*-PMMA prepolymers as the binder.

Introduction

In the past decade, considerable attention has been paid to the design and synthesis of C_{60}-containing polymers with a well-defined structure because the incorporation of C_{60}-bound molecules into polymer backbones, pendants, or the terminal groups as components may produce practically useful C_{60}-based nanomaterials having high mechanical strength and good processability while maintaining the unique physical and chemical properties of C_{60} molecules.[1,2] Among the varieties of C_{60}-containing polymers, the C_{60}-end-capped polymers are of particular interest, because the solvophobic C_{60} core self-assembles on a nanometer scale into the core−shell or vesicle-like aggregates in polar solvents.[3] Such self-assembled C_{60} aggregates are known to exhibit different photochemical and photophysical features from those of their isolated counterparts.[4] However, previous studies of the C_{60}-end-capped polymers have largely focused on their syntheses, structures, and morphology of their aggregates in solution or in the solid. Although

[†] ERATO, JST.
[‡] Nagoya University.

(1) For recent reviews of C_{60}-containing polymer materials, see: (a) Jensen, A. W.; Wilson, S. R.; Schuster, D. I. *Bioorg. Med. Chem.* **1996**, *4*, 767−779. (b) Prato, M. *J. Mater. Chem.* **1997**, *7*, 1097−1109. (c) Martín, N.; Sánchez, L.; Illescas, B.; Pérez, I. *Chem. Rev.* **1998**, *98*, 2527−2547. (d) Chen, Y.; Huang, Z.-E.; Cai, R.-F.; Yu, B.-C. *Eur. Polym. J.* **1998**, *34*, 137−151. (e) Dai, L.; Mau, A. W. H. *Adv. Mater.* **2001**, *13*, 899−913. (f) Brabec, C. J.; Sariciftci, N. S.; Hummelen, J. C. *Adv. Funct. Mater.* **2001**, *11*, 15−26. (g) Cravino, A.; Sariciftci, N. S. *J. Mater. Chem.* **2002**, *12*, 1931−1943. (h) Wudl, F. *J. Mater. Chem.* **2002**, *12*, 1959−1963. (i) Wang, C.; Guo, Z.-X.; Fu, S.; Wu, W.; Zhu, D. *Prog. Polym. Sci.* **2004**, *29*, 1079−1141. (j) Nierengarten, J.-F. *New J. Chem.* **2004**, *28*, 1177−1191.

(2) For recent examples of C_{60}-containing polymers and leading references, see: (a) Samulski, E. T.; DeSimone, J. M.; Hunt, M. O., Jr.; Menceloglu, Y. Z.; Jarnagin, R. C.; York, G. A.; Labat, K. B.; Wang, H. *Chem. Mater.* **1992**, *4*, 1153−1157. (b) Loy, D. A.; Assink, R. A. *J. Am. Chem. Soc.* **1992**, *114*, 3977−3978. (c) Shi, S.; Khemani, K. C.; Li, Q.; Wudl, F. *J. Am. Chem. Soc.* **1992**, *114*, 10656−10657. (d) Geckeler, K. E.; Hirsch, A. *J. Am. Chem. Soc.* **1993**, *115*, 3850−3851. (e) Wooley, K. L.; Hawker, C. J.; Fréchet, J. M. J. *J. Am. Chem. Soc.* **1993**, *115*, 9836−9837. (f) Hawker, C. J. *Macromolecules* **1994**, *27*, 4836−4837. (g) Taki, M.; Takigami, S.; Watanabe, Y.; Nakamura, Y.; Nishimura, J. *Polym. J.* **1997**, *29*, 1020−1022. (h) Li, J.; Yoshizawa, T.; Ikuta, M.; Ozawa, M.; Nakahara, K.; Hasegawa, T.; Kitazawa, K.; Hayashi, M.; Kinbara, K.; Nohara, M.; Saigo, K. *Chem. Lett.* **1997**, 1037−1038. (i) Ederlé, Y.; Mathis, C. *Macromolecules* **1997**, *30*, 2546−2555. (j) Xu, H.; Tang, B. Z. *J. Macromol. Sci., Pure Appl. Chem.* **1999**, *A36*, 1197−1207. (k) Samal, S.; Choi, B.-J.; Geckeler, K. E. *Chem. Commun.* **2000**, 1373−1374. (l) Zhang, F.; Svensson, M.; Andersson, M. R.; Maggini, M.; Bucella, S.; Menna, E.; Inganäs, O. *Adv. Mater.* **2001**, *13*, 1871−1874. (m) Nishimura, T.; Takatani, K.; Sakurai, S.; Maeda, K.; Yashima, E. *Angew. Chem., Int. Ed.* **2002**, *41*, 3602−3604. (n) Yamaguchi, T.; Ishii, N.; Tashiro, K. Aida, T. *J. Am. Chem. Soc.* **2003**, *125*, 13934−13935. (o) Nishimura, T.; Maeda, K.; Ohsawa, S.; Yashima, E. *Chem.—Eur. J.* **2005**, *11*, 1181−1190. (p) Fujita, N.; Yamashita, T.; Asai, M.; Shinkai, S. *Angew. Chem., Int. Ed.* **2005**, *44*, 1257−1261. (q) Ball, Z. T.; Sivula, K.; Fréchet, J. M. J. *Macromolecules* **2006**, *39*, 70−72.

10.1021/ja063252u CCC: $33.50 **© 2006 American Chemical Society**

traditional living anionic and recently developed living radical polymerizations have often been used to synthesize C_{60}-end-capped polymers with a controlled molecular weight (MW) that include, as examples, polystyrene,[3b,5] poly(methyl methacrylate) (PMMA),[5e] poly((meth)acrylic acid),[3h−j,l,6] poly(2-(dimethylamino)ethyl methacrylate),[3f,j,k] and poly(ethylene oxide),[3a,c,e] stereoregular C_{60}-end-capped polymers with a narrow molecular weight distribution (MWD) have not yet been prepared.

Recently, we reported the first synthesis, isolation, and single-molecule observation of a C_{60}-end-capped, highly isotactic PMMA (*it*-PMMA-C_{60}) with a controlled MW and a narrow MWD.[7] We anticipated that the *it*-PMMA-C_{60} might be used as an interesting component to construct supramolecular assemblies with syndiotactic (*st*-) PMMA-C_{60}, because *it*- and *st*-PMMAs are known to supramolecularly assemble to form a stereocomplex,[8−15] the structure of which is believed to be a double-stranded helix.[16] Therefore, *it*- and *st*-PMMAs having C_{60} at the controlled chain end combined with a unique self-assembly of C_{60} and a specific stereocomplex formation will provide a new sophisticated self-assembly system for constructing two- and three-dimensional arrangements of the C_{60} molecules or clusters in polymer materials.

Herein, we report a novel and versatile approach to produce the supramolecular nanospheres and nanonetworks based on *it*- and *st*-PMMA-C_{60}'s through their stereocomplex formation of the PMMA chains combined with self-assembly of the terminal C_{60} unit (Figure 1). We have found that the stereoregular PMMA-C_{60}'s self-assemble to form a core−shell aggregate with

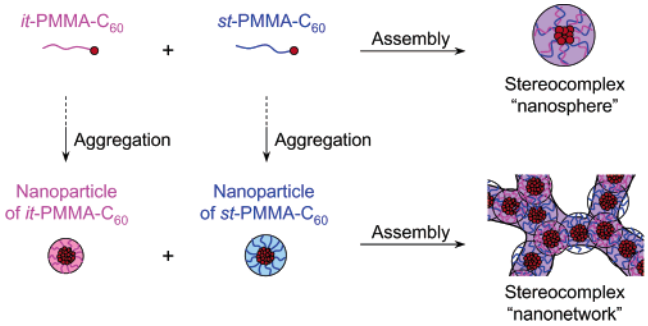

Figure 1. Schematic representation of the formations of core−shell nanospheres and nanonetworks based on *it*- and *st*-PMMA-C_{60}'s through their stereocomplex formation combined with self-assembly of the terminal C_{60}.

C_{60} as the core and the PMMA chains as the shell in a H_2O/CH_3CN (1/9, v/v) mixture, leading to uniformly sized nanoparticles, which further supramolecularly assemble into nanonetworks through iterative stereocomplex formation of the complementary PMMA chains as the shell (Figure 1). In addition, simultaneous mixing of *it*- and *st*-PMMA-C_{60}'s results in the formation of similar nanospheres (Figure 1). In these two- and three-dimensional supramolecular assembly systems, the stereocomplex formation acts as a stabilizer or binder and contributes to their significant thermal stabilities. The morphologies and thermal stabilities of the nanospheres and nanonetworks and the effect of the MW of the *it*- and *st*-PMMA-C_{60}'s on the supramolecular assemblies are also investigated.

Results and Discussion

Synthesis and Characterization of Stereoregular PMMA-C_{60}'s. The *it*- and *st*-PMMA-C_{60}'s were synthesized by the stereospecific anionic living polymerization of MMA followed by end-capping with C_{60} (Scheme 1). MMA was first living and anionically polymerized with *tert*-butylmagnesium bromide (*t*-BuMgBr) in toluene at −78 °C to give an isotactic polymer with a narrow MWD.[17] After complete consumption of the MMA, a solution of tributylaluminum (*n*-Bu_3Al) in toluene was slowly added to the *it*-PMMA living anion at −78 °C to transform the countercation,[18] and a solution of C_{60} in toluene was then added to the mixture at −78 °C, yielding *it*-PMMA-C_{60} after quenching the living polymer with CH_3OH. Its prepolymer (*it*-PMMA) was also prepared by quenching the living PMMA anion with CH_3OH (for detailed preparation procedures, see Supporting Information). Similarly, the *st*-PMMA-C_{60} was synthesized by the syndiotactic-specific anionic living polymerization of MMA with a combination of *tert*-butyllithium (*t*-BuLi) and *n*-Bu_3Al in toluene at −78 °C[19] followed by end-capping with C_{60}. The polymerization results and characteristics of the PMMA-C_{60}'s and PMMA prepolymers are summarized in Table 1. Sample codes are abbreviated using the tacticity, MW, and the end group such that *it*-35-C_{60} stands for the *it*-PMMA-C_{60} with a MW of 3500. The PMMA-C_{60}'s

(3) (a) Ederlé, Y.; Mathis, C.; Nuffer, R. *Synth. Met.* **1997**, *86*, 2287−2288. (b) Okamura, H.; Ide, N.; Minoda, M.; Komatsu, K.; Fukuda, T. *Macromolecules* **1998**, *31*, 1859−1865. (c) Taton, D.; Angot, S.; Gnanou, Y.; Wolert, E.; Setz, S.; Duran, R. *Macromolecules* **1998**, *31*, 6030−6033. (d) Wang, X.; Goh, S. H.; Lu, Z. H.; Lee, S. Y.; Wu, C. *Macromolecules* **1999**, *32*, 2786−2788. (e) Song, T.; Dai, S.; Tam, K. C.; Lee, S. Y.; Goh, S. H. *Langmuir* **2003**, *19*, 4798−4803. (f) Dai, S.; Ravi, P.; Tan, C. H.; Tam, K. C. *Langmuir* **2004**, *20*, 8569−8575. (g) Tan, C. H.; Ravi, P.; Dai, S.; Tam, K. C.; Gan, L. H. *Langmuir* **2004**, *20*, 9882−9884. (h) Tan, C. H.; Ravi, P.; Dai, S.; Tam, K. C. *Langmuir* **2004**, *20*, 9901−9904. (i) Ravi, P.; Dai, S.; Tan, C. H.; Tam, K. C. *Macromolecules* **2005**, *38*, 933−939. (j) Teoh, S. K.; Ravi, P.; Dai, S.; Tam, K. C. *J. Phys. Chem. B* **2005**, *109*, 4431−4438. (k) Ravi, P.; Dai, S.; Tam, K. C. *J. Phys. Chem. B* **2005**, *109*, 22791−22798. (l) Wang, C.; Ravi, P.; Tam, K. C. *Langmuir* **2006**, *22*, 2927−2930.
(4) Guldi, D. M.; Prato, M. *Acc. Chem. Res.* **2000**, *33*, 695−703.
(5) (a) Weis, C.; Friedrich, C.; Mülhaupt, R.; Frey, H. *Macromolecules* **1995**, *28*, 403−405. (b) Wignall, G. D.; Affholter, K. A.; Bunick, G. J.; Hunt, M. O., Jr.; Menceloglu, Y. Z.; DeSimone, J. M.; Samulski, E. T. *Macromolecules* **1995**, *28*, 6000−6006. (c) Wang, C.; He, J.; Fu, S.; Jiang, K.; Cheng, H.; Wang, M. *Polym. Bull.* **1996**, *37*, 305−311. (d) Li, L.; Wang, C.; Long, Z.; Fu, S. *J. Polym. Sci., Part A: Polym. Chem.* **2000**, *38*, 4519−4523. (e) Zhou, P.; Chen, G.-Q.; Hong, H.; Du, F.-S.; Li, Z.-C.; Li, F.-M. *Macromolecules* **2000**, *33*, 1948−1954.
(6) Yang, J.; Li, L.; Wang, C. *Macromolecules* **2003**, *36*, 6060−6065.
(7) Kawauchi, T.; Kumaki, J.; Yashima, E. *J. Am. Chem. Soc.* **2005**, *127*, 9950−9951.
(8) For reviews of PMMA stereocomplex, see: (a) Spěváček, J.; Schneider, B. *Adv. Colloid Interface Sci.* **1987**, *27*, 81−150. (b) te Nijenhuis, K. *Adv. Polym. Sci.* **1997**, *130*, 67−81. (c) Hatada, K.; Kitayama, T. *Polym. Int.* **2000**, *49*, 11−47.
(9) The PMMA stereocomplex has been applied to advanced materials, such as ultrathin films,[10] microcellular foams,[11] dialyzers,[12] thermoplastic elastomers,[13] organic−inorganic hybrid composites,[14] and ion gels.[15]
(10) (a) Serizawa, T.; Hamada, K.; Kitayama, T.; Fujimoto, N.; Hatada, K.; Akashi, M. *J. Am. Chem. Soc.* **2000**, *122*, 1891−1899. (b) Serizawa, T.; Hamada, K.; Akashi, M. *Nature (London)* **2004**, *429*, 52−55. (c) Serizawa, T.; Akashi, M. *Polym. J.* **2006**, *38*, 311−328.
(11) Mizumoto, T.; Sugimura, N.; Moritani, M.; Sato, Y.; Masuoka, H. *Macromolecules* **2000**, *33*, 6757−6763.
(12) Sugaya, H.; Sakai, Y. *Contrib. Nephrol.* **1998**, *125*, 1−8.
(13) Kennedy, J. P.; Price, J. L.; Koshimura, K. *Macromolecules* **1991**, *24*, 6567−6571.
(14) Kumar, A. A.; Adachi, K.; Chujo, Y. *J. Polym. Sci., Part A: Polym. Chem.* **2004**, *42*, 785−794.
(15) Kawauchi, T.; Kumaki, J.; Okoshi, K.; Yashima, E. *Macromolecules* **2005**, *38*, 9155−9160.
(16) Schomaker, E.; Challa, G. *Macromolecules* **1989**, *22*, 3337−3341.
(17) Hatada, K.; Ute, K.; Tanaka, K.; Okamoto, Y.; Kitayama, T. *Polym. J.* **1986**, *18*, 1037−1047.
(18) Kitayama, T.; Fujimoto, N.; Yanagida, T.; Hatada, K. *Polym. Int.* **1994**, *33*, 165−170. When the living *it*-PMMA anion initiated by *t*-BuMgBr was allowed to react with C_{60} in the absence of *n*-Bu_3Al, the functionality of C_{60} of the obtained PMMA significantly decreased (f_{C60} = 13%) probably due to the strong contact ion pairing between the Mg cations and living polymer anions.
(19) Kitayama, T.; Shinozaki, T.; Sakamoto, T.; Yamamoto, M.; Hatada, K. *Macromol. Chem., Suppl.* **1989**, *15*, 167−185.

Scheme 1. Synthesis of *it*- and *st*-*PMMA*-C_{60}'s

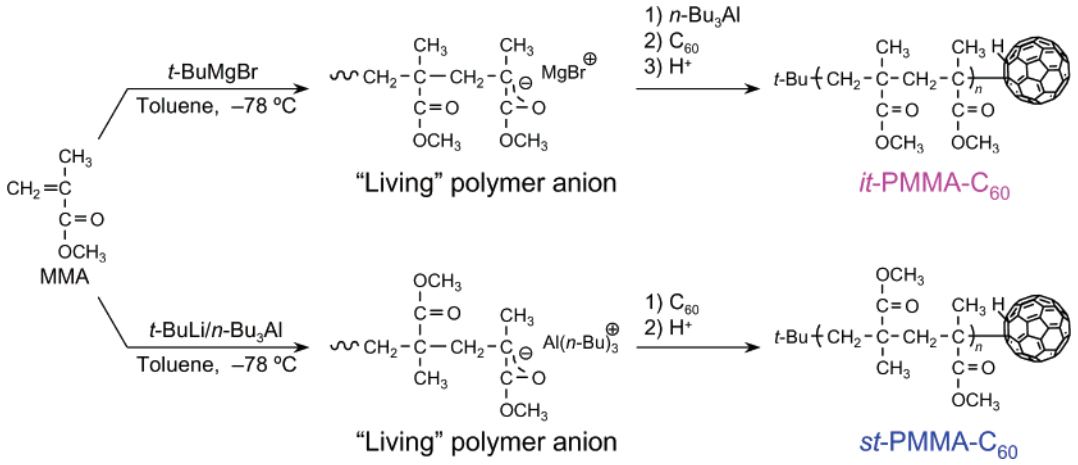

Table 1. Stereospecific Anionic Living Polymerization of MMA with Organometallic Initiators in Toluene at −78 °C[a]

					polymer						
							tacticity (%)[c]				
run	initiator	[M]/[I]	time (day)	C_{60} in feed (mmol)	$\bar{M}n$[b]	$\bar{M}w/\bar{M}n$[b]	mm	mr	rr	f_{C60}[d] (%)	sample code
1	*t*-BuMgBr	30	1	−	3500	1.19	96	4	0	−	*it*-35
2		30	1	0.29	3500	1.20	96	4	0	62	*it*-35-C_{60}
3		200	20	−	21800	1.12	97	3	0	−	*it*-218
4		200	20	0.12	22900	1.12	97	3	0	66	*it*-229-C_{60}
5	*t*-BuLi/*n*-Bu_3Al	30	1	−	5400	1.11	1	10	89	−	*st*-54
6		30	1	0.29	5300	1.12	1	9	90	70	*st*-53-C_{60}
7		200	14	−	37800	1.18	1	9	90	−	*st*-378
8		200	14	0.12	36000	1.21	1	9	90	63	*st*-360-C_{60}

[a] MMA, 6 mmol; toluene, 6 mL; yield, 100%. [b] Determined by SEC. PMMA standards were used for the calibration. [c] Determined from ^{13}C NMR signals due to the carbonyl carbon. [d] Functionality of C_{60} estimated on the basis of the absorbance at 330 nm in its UV−vis spectrum (see Figure S-1 in Supporting Information).

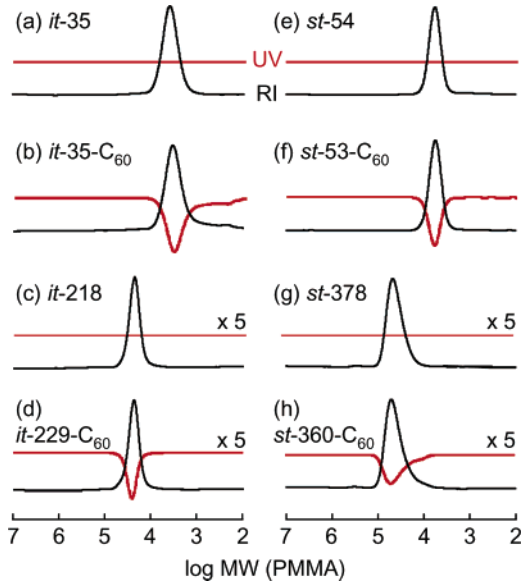

Figure 2. RI (black line) and UV (330 nm, red line) detected SEC curves of *it*-35 (a), *it*-35-C_{60} (b), *it*-218 (c), *it*-229-C_{60} (d), *st*-54 (e), *st*-53-C_{60} (f), *st*-378 (g), and *st*-360-C_{60} (h) using $CHCl_3$ as the eluent.

and their prepolymers were analyzed by size exclusion chromatography (SEC) using refractive index (RI) and UV (330 nm) dual detectors with $CHCl_3$ as the eluent (Figure 2). Apparently, the PMMA prepolymers (a, c, e, and g) showed unimodal SEC curves detected only by RI, while the PMMA-C_{60}'s having a chromophoric C_{60} unit at the terminal end exhibited similar SEC curves detected by both RI and UV (b, d, f, and h); the MWDs remained unimodal and narrow, indicating that the reactions of the living polymer with C_{60} proceeded bimolecularly without the formation of bisadducts. The functionality of C_{60} (f_{C60}) values of the PMMA-C_{60}'s were estimated by their absorption spectra on the basis of the molar absorptivity (ϵ) at 330 nm of a model compound of the PMMA-C_{60}'s (MIB-C_{60}, $(CH_3)_2C(CO_2CH_3)$-C_{60}-H)[7] (Figure S-1 in Supporting Information). Both the PMMA-C_{60}'s and MIB-C_{60} showed a sharp absorption band at around 434 nm which is a characteristic band for the C_{60} derivatives with two organic groups attached at the 1,2-positions of the 6,6-juncture bond,[20] indicating that the addition of the PMMA living anion to C_{60} occurs at the 6,6-juncture of C_{60}. The estimated f_{C60} values were not very high (f_{C60} = 62−70% in Table 1), probably due to the low reactivity of the living PMMA enolate anion toward C_{60} at −78 °C.

The structures including the chain-end structure of low MW PMMA-C_{60}'s (*it*-35-C_{60} and *st*-53-C_{60}) were fully characterized by one- (1D) and two-dimensional (2D) ^1H and ^{13}C NMR, matrix-assisted laser desorption ionization time-of-flight mass (MALDI-TOF-MS) and MS−MS spectroscopies. Figure 3 shows the typical, fully assigned 1D NMR and MALDI-TOF-MS spectra of *it*-35-C_{60} (for the characterizations of *st*-53-C_{60} and MIB-C_{60}, see Figures S-2−6 in Supporting Information).

(20) Okamura, H.; Murata, Y.; Minoda, M.; Komatsu, K.; Miyamoto, T.; Wan, T. S. M. *J. Org. Chem.* **1996**, *61*, 8500−8502.

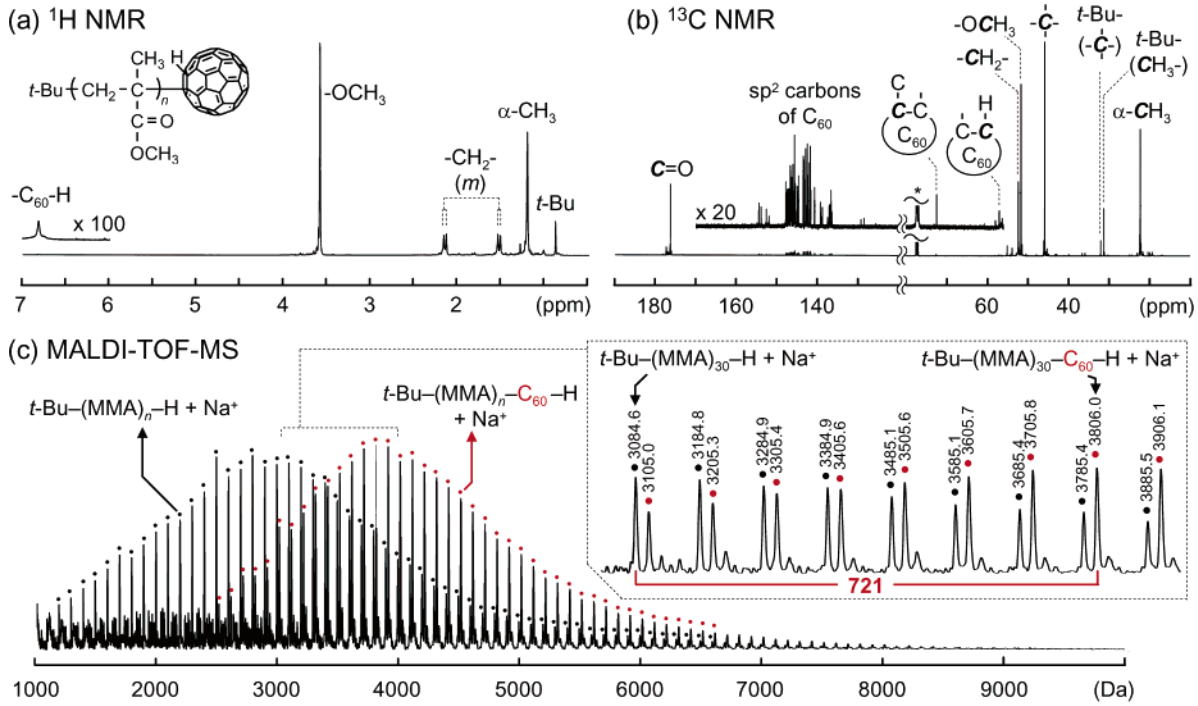

Figure 3. (a) ^{1}H NMR, (b) ^{13}C NMR, and (c) MALDI-TOF-MS spectra of *it*-35-C_{60}. The NMR spectra were measured in $CDCl_3$ at 55 °C. The MS measurement was performed using dithranol as a matrix and sodium trifluoroacetate as a cationizing agent.

The *it*-35-C_{60} exhibited characteristic resonances for the C_{60}-bonded proton (6.8 ppm as a broadened peak) (Figure 3a) and the proton- and PMMA-bonded sp^3 carbons as well as the sp^2 carbons of the terminal C_{60} unit (56.8, 72.3, and 125−155 ppm, respectively) (Figure 3b) in its ^{1}H and ^{13}C NMR spectra, respectively. The correlation peak between the proton signal at 6.8 ppm and the carbon signal at 56.8 ppm in the heteronuclear single-quantum correlation (HSQC) spectrum (Figure S-4b in Supporting Information) together with a comparison with the corresponding spectra of MIB-C_{60} (Figures S-2 and -3 in Supporting Information) were used for the assignments.

In the MALDI-TOF-MS spectrum of *it*-35-C_{60} (Figure 3c), two series of peaks (black and red circles), whose interval was regular and separated by 100 Da corresponding to the molar mass of the MMA monomer were observed. The masses of the black circle peaks are equal to the MWs of *t*-Bu-(MMA)$_n$-H combined with a sodium ion from the cationizing reagent, while those of the red circle peaks shifted by 721 Da from the black circle peaks, corresponding to a C_{60} molar mass, are equal to the MWs expected for *t*-Bu-(MMA)$_n$-C_{60}-H combined with a sodium ion.[21] The further MS−MS analysis of a PMMA-C_{60} peak revealed the loss of a C_{60} molar mass as the fragmentation peak (Figure S-6 in Supporting Information), clearly indicating that one C_{60} unit was covalently attached to the polymer chain end.

Self-Assembly of *it*- and *st*-PMMA-C_{60}'s into Nanoparticles in Polar Solvent. C_{60}-based amphiphilic derivatives[22] and polymers[3] are known to form self-assembled clusters in polar solvents due to their solvophobic characteristics. We previously demonstrated that this peculiar feature could be used to isolate a monosubstituted C_{60}-end-capped, high MW *it*-PMMA (M_n = 115 000) using a CH_3OH/tetrahydrofuran (THF) (3/7, v/v) mixture as the aggregation solvent, although the aggregation process was time-dependent and required a rather long time in the solvent mixture.[7] We then applied this assembly methodology to the construction of supramolecular nanospheres and nanonetworks based on self-assembled C_{60} clusters using *it*- and *st*-PMMA-C_{60}'s through their stereocomplex formation. We found that the *it*- and *st*-PMMA-C_{60}'s prepared in this study also self-assembled into C_{60} clusters in CH_3CN, which is a strongly stereocomplexing solvent,[8a,23] in the presence of H_2O (H_2O/CH_3CN = 1/9, v/v). Figure 4A shows the RI- and UV-detected SEC curves of the *it*- and *st*-PMMA-C_{60} solutions together with the PMMA prepolymers after the samples had been allowed to stand for 96 h in the solvent mixture ([PMMA] = 2 mg/mL). The apparent MWs of PMMA-C_{60}'s detected by the RI and UV shifted toward extremely high MWs on the order 10^8−10^9, and the shifts in the UV trace were significant (b, d, f, and h in Figure 4A). These results indicate that the PMMA-C_{60}'s self-aggregate into large clusters with C_{60} as the core and the polymer chain as the shell,[3] while the unreacted PMMAs exist as individual polymer chains, because the PMMA prepolymers showed no aggregation under identical conditions (a, c, e, and g in Figure 4A). The aggregation processes were time-dependent and required a long time in the solvent mixture (Figure S-7 in Supporting Information). However, interestingly, the aggregation rate was found to be highly influenced by the

(21) The two series of peaks in the MALDI-TOF-MS spectra suggest incomplete functionalization of the PMMA terminal ends with C_{60}, but the differences in signal intensities cannot be used to determine the f_{C60} due to differences in ionization efficiency of the two polymers with significantly different end groups. See: Peacock, P. M.; McEwan, C. N. *Anal. Chem.* **2004**, *76*, 3417−3427.

(22) For recent reviews of supramolecular assembly of amphiphilic C_{60} molecules, see: (a) Korobov, M. V.; Smith, A. L. In *Fullerenes: Chemistry, Physics, and Technology*; Kadish, K. M., Ruoff, R. S., Eds.; Wiley: New York, 2000; pp 53−89. (b) Nakamura, E.; Isobe, H. *Acc. Chem. Res.* **2003**, *36*, 807−815. (c) Guldi, D. M.; Zerbetto, F.; Georgakilas, V.; Prato, M. *Acc. Chem. Res.* **2005**, *38*, 38−43 and references therein.

(23) Vorenkamp, E. J.; Bosscher, F.; Challa, G. *Polymer* **1979**, *20*, 59−64.

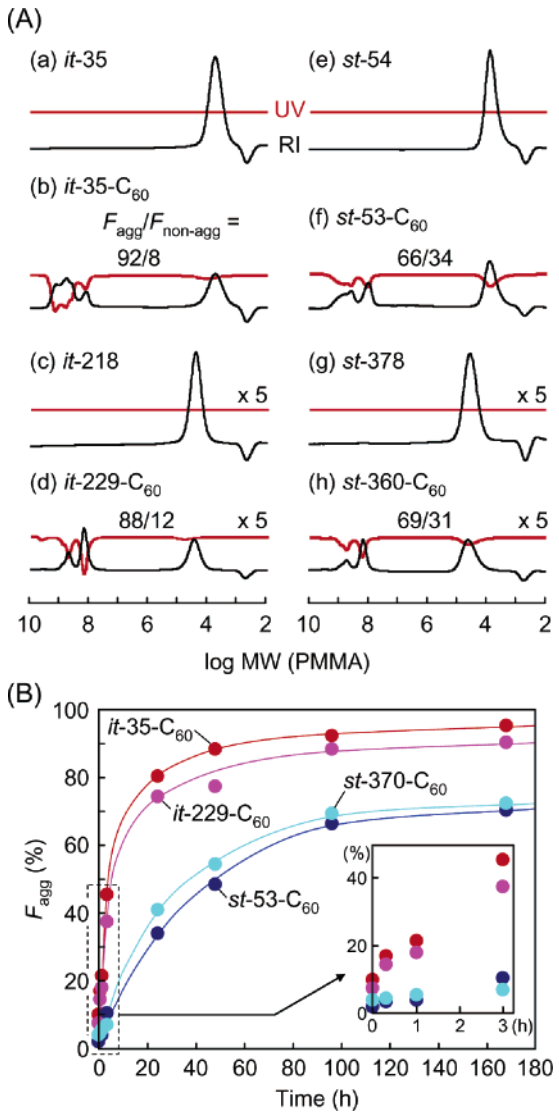

Figure 4. (A) RI (black line) and UV (330 nm, red line) detected SEC curves of *it*-35 (a), *it*-35-C_{60} (b), *it*-218 (c), *it*-229-C_{60} (d), *st*-54 (e), *st*-53-C_{60} (f), *st*-378 (g), and *st*-360-C_{60} (h) using H_2O/CH_3CN (1/9, v/v) as the eluent. The SEC curves were obtained after the samples had been allowed to stand at room temperature for 96 h in H_2O/CH_3CN (1/9, v/v) ([PMMA] = 2 mg/mL). Peak area ratios of aggregated (F_{agg}) and nonaggregated ($F_{non-agg}$) PMMA-C_{60}'s detected by UV in SEC curves are shown in (b), (d), (f), and (h). (B) Changes in the aggregated *it*- and *st*-PMMA-C_{60}'s fraction (F_{agg}) with time. The F_{agg} values were estimated based on the UV (330 nm) detected SEC peak areas of the aggregated (F_{agg}) and nonaggregated ($F_{non-agg}$) PMMA-C_{60} in H_2O/CH_3CN (1/9, v/v) (see also Figure S-7 in Supporting Information). (Inset) Details of the time-dependent F_{agg} changes.

tacticity of the polymer chains; *it*-PMMA-C_{60}'s tended to aggregate more rapidly and efficiently than *st*-PMMA-C_{60}'s, and this tendency was almost independent of the MW of the PMMAs (Figure 4B). The changes in the UV-detected SEC peak areas of the aggregated (F_{agg}) and nonaggregated ($F_{non-agg}$) PMMA-C_{60}'s with time (Figure 4B) show that, for example, 92% of *it*-35-C_{60} was involved in the aggregates after storing the sample for 96 h, while 66% of *st*-53-C_{60} aggregated under the same conditions (b and f in Figure 4A, respectively). It has been known that *it*- and *st*-PMMAs assume a different conformation depending on the solvents,[24] and this difference dependence in their conformations may result in the difference in the aggregation rate between *it*- and *st*-PMMA-C_{60}'s.

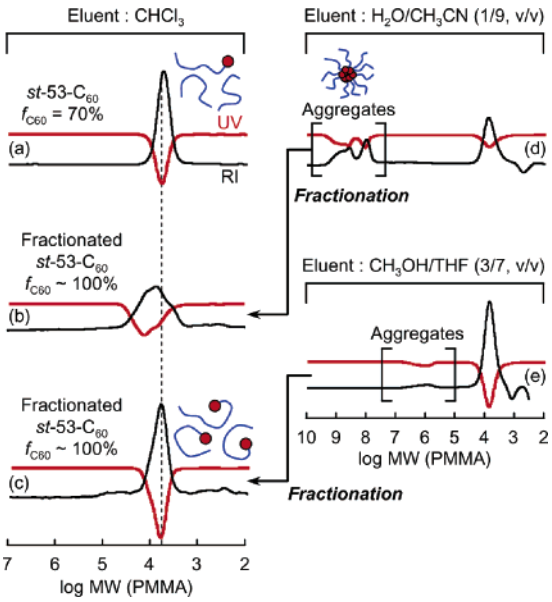

Figure 5. RI (black line) and UV (330 nm, red line) detected SEC curves of *st*-53-C_{60} before (f_{C60} = 70%) (a, d) and after ($f_{C60} \approx$ 100%) (b, c) purification by SEC fractionation using $CHCl_3$ (a−c), H_2O/CH_3CN (1/9, v/v) (d), and CH_3OH/THF (3/7, v/v) (e) as the eluent. The SEC curves (d, e) were obtained after the samples had been allowed to stand at room temperature for 96 h. The fractions marked by brackets in (d) and (e) were collected and then injected into the SEC system (b) and (c), respectively.

The aggregate formations of the PMMA-C_{60}'s were also supported by changes in their UV−vis spectra in H_2O/CH_3CN (1/9, v/v) with time; the absorption bands became quite broadened after 96 h (Figure S-8 in Supporting Information) as observed in analogous C_{60} derivatives in polar solvents.[25]

As previously reported, completely C_{60}-end-capped *it*-PMMAs could be isolated through self-assembly by SEC fractionation using a polar solvent as the eluent, even when the functionality of C_{60} was low.[7] The *st*-53-C_{60} aggregates were then fractionated by SEC using H_2O/CH_3CN (1/9, v/v) as the eluent and subjected to the SEC system using $CHCl_3$ as the eluent (b and d of Figure 5). The fractionated aggregates revealed a rather broad SEC curve, indicating that the aggregates formed in the H_2O/CH_3CN did not dissociate in $CHCl_3$. In contrast, the aggregates formed in a CH_3OH/THF (3/7, v/v) mixture were found to dissociate into individual polymers in $CHCl_3$ as evidenced by the nearly identical, unimodal RI and UV SEC curves with a narrow MWD as observed for *st*-53-C_{60} before the self-aggregation (c and e of Figure 5), although the recovery yield was very low. On the basis of the intensity ratio of the RI and UV traces, the f_{C60} values of the isolated *st*-53-C_{60}'s were estimated to be almost 100%. Although the completely C_{60}-end-capped PMMAs could be isolated by self-assembly of the C_{60} units followed by SEC fractionation, the "as-prepared" PMMA-C_{60}'s were used for further supramolecular assembly experiments based on stereocomplex formation, because the functionalities of C_{60} of the PMMA-C_{60}'s before isolation (f_{C60} > 60%) may be sufficiently high.

(24) Wunderlich, W. In *Polymer Handbook*, 4th ed.; Brandrup, J., Immergut, E. H., Grulke, E. A., Eds.; Wiley: New York, 1999; pp V87−V90.
(25) (a) Bensasson, R. V.; Bienvenue, E.; Dellinger, M.; Leach, S.; Seta, P. *J. Phys. Chem.* **1994**, *98*, 3492−3500. (b) Felder, D.; Guillon, D.; Lévy, R.; Mathis, A.; Nicoud, J.-F.; Nierengarten, J.-F.; Rehspringer, J.-L.; Schell, J. *J. Mater. Chem.* **2000**, *10*, 887−892. (c) Angelini, G.; Maria, P. D.; Fontana, A.; Pierini, M. *Langmuir* **2001**, *17*, 6404−6407.

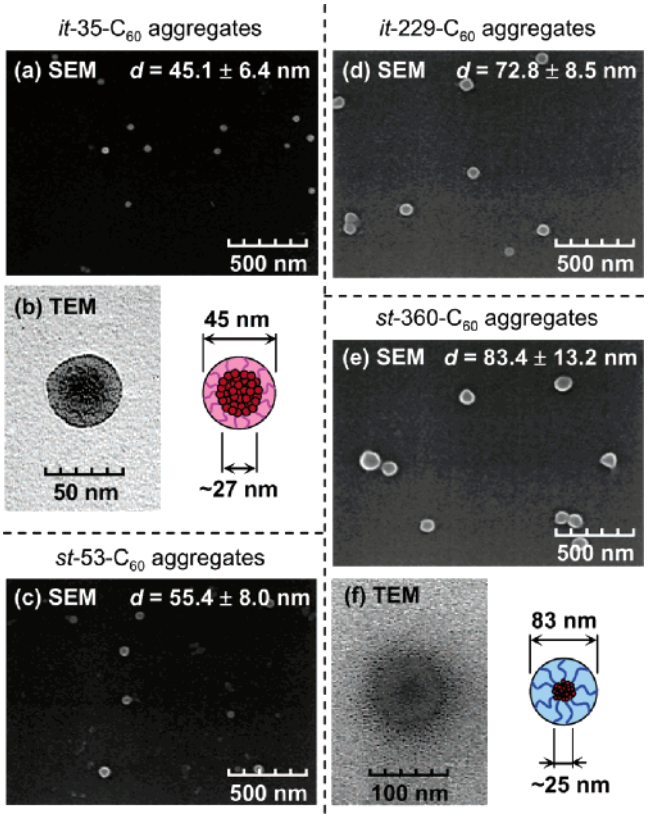

Figure 6. SEM (a, c, d, e) and TEM (b, f) images of *it*-35-C_{60} (a, b), *st*-53-C_{60} (c), *it*-229-C_{60} (d), and *st*-360-C_{60} (e, f) cast from solutions in H_2O/CH_3CN (1/9, v/v) on mica (a, c−e) or TEM grid precoated with poly(vinyl formal) (b, f). The solutions were allowed to stand at room temperature for 96 h before measurements. The TEM images were taken without staining and the black areas indicate C_{60}-rich regions.

Next, we investigated the size and morphology of the self-aggregated PMMA-C_{60}'s formed in the H_2O/CH_3CN (1/9, v/v) mixture by field emission scanning electron microscopy (SEM) and transmission electron microscopy (TEM) (Figure 6). The SEM images revealed the presence of uniformly sized spherical nanoparticles composed of a core−shell structure, whose average diameters increased with the increasing MW of the PMMA chains from ca. 45 and 55 nm for *it*-35-C_{60} and *st*-53-C_{60} to ca. 73 and 83 nm for *it*-229-C_{60} and *st*-360-C_{60}, respectively. These values are almost comparable to those estimated by dynamic light scattering (DLS) analysis of the aggregates in H_2O/CH_3CN (1/9, v/v) (Figure S-9 in Supporting Information). The double logarithmic plot between the MW of the PMMA-C_{60} chains and the diameters of the nanoparticles or aggregates estimated by the SEM and DLS measurements, respectively, gave an almost straight line, suggesting that the particle sizes (d) appear to depend on the MW of the PMMA-C_{60} chains as such $d \approx MW^{1/3}$ (data not shown). This means that the same number of PMMA-C_{60} chains irrespective of their MW may self-aggregate into nanoparticles with a different size but with the same C_{60} core diameter. We then performed TEM observations of the nanoparticles without staining. The TEM images of *it*-35-C_{60} and *st*-360-C_{60} aggregates revealed a core−shell structure with C_{60} as the core of ca. 27 and 25 nm diameter and a PMMA shell thickness of ca. 9 and 29 nm, respectively (Figure 6, b and f). The observed C_{60} core diameters were roughly the same irrespective of the large difference in their particle sizes (45 and 83 nm). These TEM observations also support the structure of the self-aggregated nanoparticles.

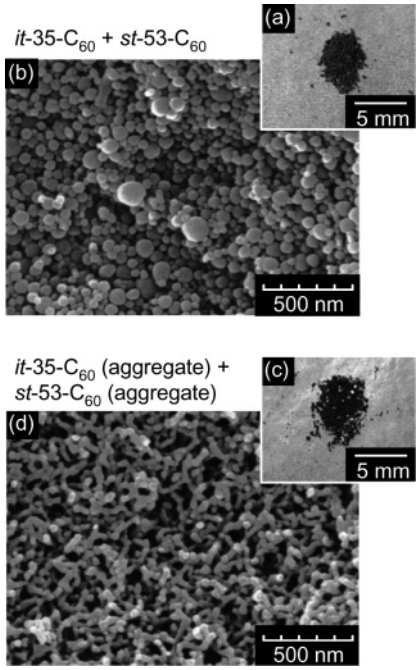

Figure 7. Photographs (a, c) and SEM images (b, d) of stereocomplexes between *it*-35-C_{60} and *st*-53-C_{60} (a, b), and *it*-35-C_{60} (aggregate) and *st*-53-C_{60} (aggregate) (c, d) obtained from H_2O/CH_3CN (1/9, v/v) solutions (*it*/*st* = 1/2); the polymer concentration was 2 mg/mL.

Stereocomplex Formation between *it*- and *st*-PMMA-C_{60}'s. Stereocomplex formation of *it*- and *st*-PMMA-C_{60}'s in the H_2O/CH_3CN (1/9, v/v) mixture before self-assembly of the C_{60}-end-capped PMMAs was first investigated; CH_3CN is a typical strong stereocomplexing solvent.[8a,23] Solutions of *it*-35-C_{60} and *st*-53-C_{60} in H_2O/CH_3CN (1/9, v/v) at a polymer concentration of 2 mg/mL were separately prepared and mixed at a ratio of *it*/*st* = 1/2 in unit molar base immediately after the sample preparations.[26] A dark-brown solid was obtained by evaporating the solvents in a stream of nitrogen followed by drying under vacuum at room temperature (Figure 7a). Differential scanning calorimetry (DSC) measurements indicated the stereocomplex formation; the obtained solid exhibited a sharp endothermic peak at 147.3 °C, which is a characteristic peak for the melting of the stereocomplexed PMMA as evidenced by a similar melting peak for a blend of *it*-35 and *st*-54 prepared under the same conditions (a and b in Figure S-10 in Supporting Information). The SEM image of the stereocomplex of the *it*-35-C_{60} and *st*-53-C_{60} revealed the formation of spherical nanoparticles (Figure 7b). Similar spherical-like morphology was also observed for the stereocomplex prepared from higher MW PMMA-C_{60}'s, *it*-229-C_{60} and *st*-360-C_{60} under the same conditions (Figure S-11b in Supporting Information), whereas no regular structure could be observed in the SEM image of the stereocomplex between the corresponding PMMA prepolymers, *it*-35 and *st*-54 (Figure S-11a in Supporting Information). Although similar nanoparticles could be obtained from self-aggregation of *it*- or *st*-PMMA-C_{60}'s in H_2O/CH_3CN (1/9, v/v) (Figure 6), the formation required a long time in the mixed solvent. In sharp contrast,

(26) It is generally accepted that the stereocomplex of *it*- and *st*-PMMAs quantitatively forms at the stoichiometric ratio of *it*/*st* = 1/2.[8,15,16,23]

the present assembly method based on stereocomplexation required no such aging time and likely produces nanoparticles with a core−shell structure through self-assembly of the C_{60} units and stereocomplex formation of the *it*- and *st*-PMMA chains which may take place at once, or the latter may accelerate the former. In addition, the supramolecularly cross-linked nanoparticles through stereocomplex formation were found to be more thermally stable than the self-aggregated PMMA-C_{60} nanoparticles as observed by SEM measurements of each sample after heat treatment (Figure S-12, a and b, in Supporting Information). The *it*-35-C_{60} self-aggregated nanoparticles melted at 80 °C, while the stereocomplexed nanoparticles formed between the *it*-35-C_{60} and *st*-53-C_{60} maintained their spherical structures even at 120 °C and finally melted above 140 °C, demonstrating the advantage of supramolecular stereocomplex formation in the design of robust nanostructures.

Next, we studied the stereocomplex formation between spherical *it*- and *st*-PMMA-C_{60}'s aggregates. The core−shell aggregates of *it*-35-C_{60} and *st*-53-C_{60} were separately prepared after the samples had been allowed to stand for 96 h in H_2O/CH_3CN ([PMMA] = 2 mg/mL) in the same way as described above. Upon mixing the *it*- and *st*-PMMA-C_{60} aggregate solutions (*it*/*st* = 1/2), a dark brown powder was obtained after evaporating the solvents followed by drying under vacuum at room temperature (Figure 7c). The DSC thermogram of the aggregates indicated the stereocomplex formation, thus showing a melting peak at 145.5 °C (Figure S-10c in Supporting Information). The size and morphology of the stereocomplexed aggregates in the bulk state were then investigated by SEM. Interestingly, the stereocomplex exhibited a continuous three-dimensional (3D) nanonetwork with a width of ca. 50 nm in which the self-assembled *it*- and *st*-PMMA-C_{60} clusters were robustly connected with a 3D arrangement through interpenetrative stereocomplex formation (Figure 7d).[27] The stereocomplex between self-assembled *it*-35-C_{60} and *st*-53-C_{60} clusters also maintained their network structures even at 120 °C due to the improvement of thermal stability by the stereocomplex formation (Figure S-12c in Supporting Information). Stereocomplexation between self-assembled higher MW *it*- and *st*-PMMA-C_{60} clusters, *it*-229-C_{60} and *st*-360-C_{60} aggregates also produced a 3D nanonetwork having a greater width of ca. 80 nm than that of the stereocomplex formed between the *it*-35-C_{60} and *st*-53-C_{60} clusters (Figure S-11c in Supporting Information). Similar nanonetwork architectures can be created using *it*-PMMA-C_{60} clusters and *st*-PMMA prepolymers as a binder (Figure S-11, d and e, in Supporting Information). These results demonstrate that supramolecular nanospheres and nanonetworks can be rationally created using *it*- and *st*-PMMA-C_{60}'s through their stereocomplex formation combined with self-assembly of the terminal C_{60}, in which the stereocomplex formation acts as a robust binder. To obtain more detailed information on the structures and morphologies of the nanoarchitectures based on *it*- and *st*-PMMA-C_{60}'s, two-dimensional (2D) nanospheres and nanonetworks were prepared under dilute conditions, and their structures and morphologies were investigated by SEM.

Two-Dimensional Nanostructures of Stereocomplexes between *it*- and *st*-PMMA-C_{60}'s. Dilute solutions of *it*- and *st*-PMMA-C_{60}'s with different MWs in H_2O/CH_3CN (1/9, v/v) at a polymer concentration of 0.2 mg/mL were separately prepared and mixed at a ratio of *it*/*st* = 1/2 in unit molar base immediately after the sample preparations. At the low concentration, macroscopic phase separation or clouding of the solutions hardly occurred. The SEM images of the stereocomplexes between *it*- and *st*-PMMA-C_{60}'s revealed the presence of uniformly sized spherical nanoparticles (Figure 8, b and c), while no regular structure could be observed in the SEM image of the stereocomplex of the corresponding PMMA prepolymers, *it*-35 and *st*-54 (Figure 8a). These results indicate that not only stereocomplex formation but also self-aggregation of the terminal C_{60} units plays a crucial role in the regular nanoparticle formation. The average diameters of the stereocomplex nanospheres increased with the increasing MW of the PMMA chains from ca. 82 nm (*it*-35-C_{60} and *st*-53-C_{60}) to ca. 102 nm (*it*-229-C_{60} and *st*-360-C_{60}), and these values are larger than those of the corresponding self-assembled C_{60} clusters (Figure 6), suggesting possible control of the nanoparticle size by altering the aggregation method and the MW of the PMMA chains.

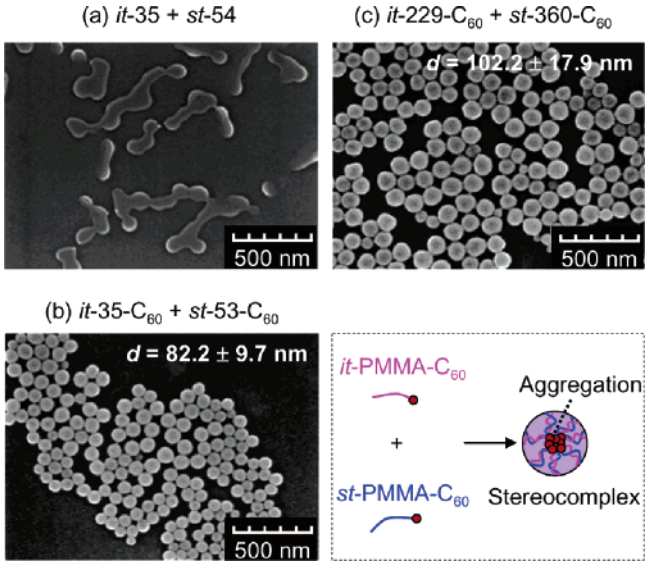

Figure 8. SEM images of stereocomplexes between *it*-35 and *st*-54 (a), *it*-35-C_{60} and *st*-53-C_{60} (b), and *it*-229-C_{60} and *st*-360-C_{60} (c) cast from H_2O/CH_3CN (1/9, v/v) solutions on mica after immediately mixing each sample solution (*it*/*st* = 1/2); the polymer concentration was 0.2 mg/mL.

Two-dimensional network structures were also prepared and investigated by SEM. The self-assembled *it*-35-C_{60} and *st*-53-C_{60} clusters were separately prepared in H_2O/CH_3CN at a polymer concentration of 2 mg/mL in the same way as described above. After diluting the PMMA-C_{60} aggregate solutions (0.2 mg/mL), they were immediately mixed at the ratio of *it*/*st* = 1/2 in unit molar base to produce 2D interpenetrative networks. Figure 9 shows the SEM images of the stereocomplexes formed between *it*- and *st*-PMMA-C_{60}'s aggregates with different diameters; 2D nanoscale network structures were clearly observed. The average widths of the net appeared to reflect the size of the original self-assembled PMMA-C_{60} clusters and increased with an increase in the cluster size, suggesting that the core−shell aggregates of the *it*- and *st*-PMMA-C_{60}'s further self-assembled with each other into 2D and 3D nanonetworks through iterative stereocomplex formation of the PMMA chains

(27) For supramolecular C_{60}-based polymeric nanonetwork formations, see: (a) Liu, Y.; Wang, H.; Liang, P.; Zhang, H.-Y. *Angew. Chem., Int. Ed.* **2004**, *43*, 2690−2694. (b) Haino, T.; Matsumoto, Y.; Fukazawa, Y. *J. Am. Chem. Soc.* **2005**, *127*, 8936−8937.

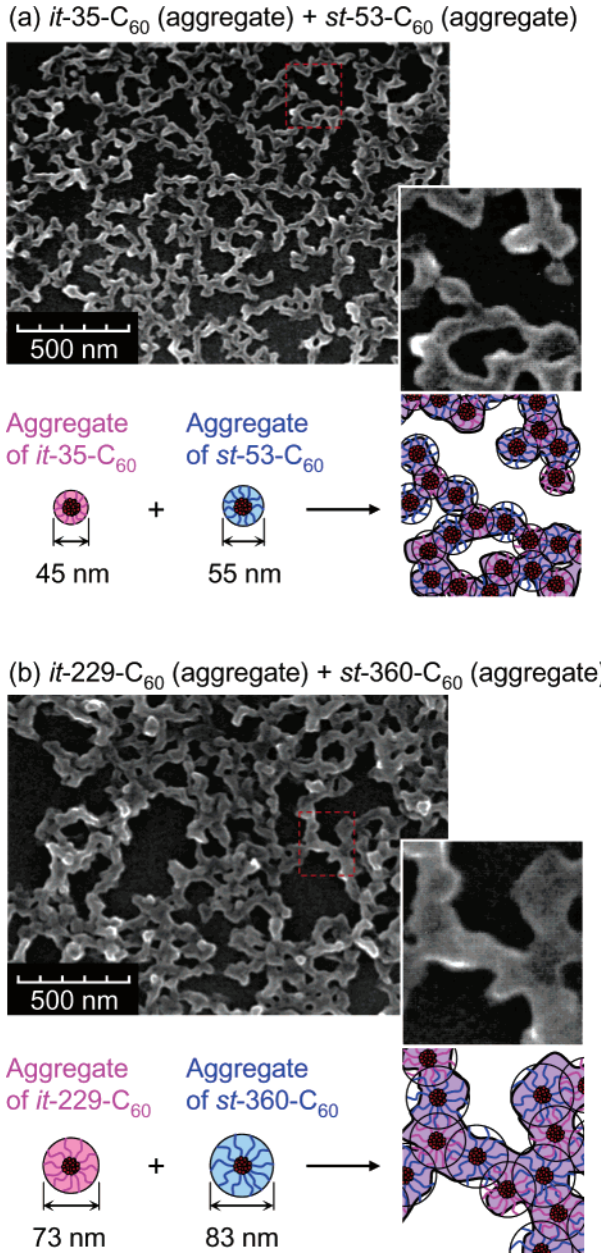

Figure 9. SEM images of stereocomplexes between *it*-35-C_{60} (aggregate) and *st*-53-C_{60} (aggregate) (a), *it*-229-C_{60} (aggregate) and *st*-360-C_{60} (aggregate) (b) cast from H_2O/CH_3CN (1/9, v/v) solutions (*it*/*st* = 1/2) on mica; the polymer concentration was 0.2 mg/mL. Magnified SEM images corresponding to the area indicated by dotted squares in (a) and (b) are also shown together with schematic representations of the nanonetworks.

as the shell, depending on the concentration of the PMMA-C_{60} clusters.[28] This methodology may be applicable to produce unique C_{60}-containing polymer materials with two- and three-dimensionally controlled arrangements of the self-assembled C_{60} clusters.

(28) The effect of the molar ratio of the self-assembled *it*-35-C_{60} and *st*-53-C_{60} aggregates on 2D nanonetwork formations was also investigated. The SEM images of the stereocomplexes formed between *it*/*st* = 1/2, 1/1, and 2/1 in unit molar base revealed the similar 2D nanonetwork formations, but their network sizes were significantly different from each other, depending on the molar ratio (Figure S-13, b−d, in Supporting Information). On the other hand, when the *it*- and *st*-PMMA aggregates were mixed at the ratio of *it*/*st* = 1/4 and 4/1, the stereocomplex formation did not take place efficiently, and oligomeric aggregates were produced, probably because the excess complementary PMMA aggregates may terminate the propagation of the network formation (Figure S-13, a and e, in Supporting Information).

Similar nanonetworks can also be created through stereocomplex formation of either a self-assembled *it*- or *st*-PMMA-C_{60} cluster with its complementary PMMA prepolymer, in which the PMMA prepolymer acts as a binder interconnecting the PMMA-C_{60} clusters. For example, stereocomplexation between the self-assembled *it*-35-C_{60} aggregate and *st*-PMMA prepolymers with different MWs, *st*-54 and *st*-378 in H_2O/CH_3CN (1/9, v/v) solution ([PMMA] = 0.2 mg/mL) produced oligomeric aggregates and 2D networks, respectively (Figure S-14 in Supporting Information). These differences in the morphology of the interconnected structure seem to be ascribed to the difference in the MW of the *st*-PMMA prepolymers. Under dilute conditions, low MW *st*-PMMAs predominantly bind to a single *it*-35-C_{60} aggregate, while high MW *st*-PMMAs are long enough to interconnect the *it*-35-C_{60} aggregates, resulting in the nanonetwork structure even at low concentrations. However, at high concentrations, PMMA chains can efficiently serve as the binder independent of the MW. Therefore, 3D nanonetworks were produced upon mixing the *it*-35-C_{60} aggregates and low (*st*-54) and high (*st*-378) MW *st*-PMMAs in H_2O/CH_3CN (1/9, v/v) followed by evaporating the solvents (Figure S-11, d and e, in Supporting Information).

Conclusions

In summary, we have demonstrated that the C_{60}-end-capped highly stereoregular *it*- and *st*-PMMAs with a narrow MWD can be used as a versatile component to construct uniformly sized nanospheres and nanonetworks based on a unique and specific supramolecular assembly, stereocomplex formation between the *it*- and *st*-PMMA chains combined with solvophobic interaction-driven self-assembly of the terminal C_{60}. The stereocomplexation not only produced 2D and 3D arrangements of self-assembled C_{60} clusters but also thermally stabilized the nanospheres and nanonetworks. In addition, the morphologies of the nanospheres and nanonetworks including the size and width, respectively, can be controlled by altering the MWs of the PMMAs. The present assembly methodology developed here will provide useful electrooptic materials, and work along this line is now in progress.

Experimental Section

Full experimental details are available in the Supporting Information.

Acknowledgment. We are deeply grateful to Dr. S. Arai (EcoTopia Science Research Center, Nagoya University) for TEM observations.

Supporting Information Available: Experimental details, UV−vis, ^1H NMR, ^{13}C NMR, HSQC, MALDI-TOF-MS, and MS−MS spectra of PMMA-C_{60}'s, time-dependent SEC and UV−vis changes of PMMA-C_{60}'s in H_2O/CH_3CN (1/9, v/v), DLS results of PMMA-C_{60} aggregates in H_2O/CH_3CN (1/9, v/v), DSC thermograms and SEM images of stereocomplexes between *it*- and *st*-PMMA-C_{60}'s, changes in the morphology of *it*-PMMA-C_{60} self-aggregates and stereocomplexes between *it*- and *st*-PMMA-C_{60}'s before and after heat treatment, SEM images of stereocomplexes between *it*- and *st*-PMMA-C_{60} aggregates at several mixing ratios, and SEM images of stereocomplexes between *it*-PMMA-C_{60} aggregates and *st*-PMMAs with different MWs. This material is available free of charge via the Internet at http://pubs.acs.org.

JA063252U